# Selective Growth of Cobalt Nanoclusters in Domains of Block Copolymer Films

J. I. Abes,† R. E. Cohen,*,† and C. A. Ross‡

*Departments of Chemical Engineering and Materials Science and Engineering, and the Center for Materials Science and Engineering, Massachusetts Institute of Technology, Cambridge, Massachusetts 02139*

*Received October 16, 2002. Revised Manuscript Received December 24, 2002*

We have produced, by thermal decomposition of an organometallic complex in a bulk film of P(S-*b*-2VP), nonagglomerated cobalt nanoparticles that exhibit significant room-temperature magnetic coercivity. The particles are patterned on the nanoscale: they reside within the P2VP domains of the block copolymer morphology. These results are made possible by the selective sequestration of the organometallic complex into these domains in amounts sufficient to nucleate and grow substantial quantities of cobalt nanoparticles that are larger than the size required for ferromagnetic behavior. The in situ synthesis of ferromagnetic nanoparticles selectively inside the P2VP domains of P(S-*b*-2VP) block copolymer films has been demonstrated.

## Introduction

The synthesis of metallic nanoparticles has been the subject of research in a wide range of fields, including surface catalysis,[1−6] selective light absorption,[5,7,8] and electronics.[7,9,10] Due to their unusual magnetic properties, and their applicability to high-density magnetic memory, magnetic nanoparticles have been, and continue to be, of great interest. Synthesis methods in the literature include sonication,[11−14] sputtering,[15−17] performing reactions on ions sequestered in polyelectrolyte films,[9,18−25] and growth within micelles.[2−5,26−36] A large number of papers exist regarding particles that are superparamagnetic at room temperature.[11,14,18−22,24,28,33,37−40] Reaching the com-

* Corresponding author.
‡ Department of Materials Science and Engineering.
† Department of Chemical Engineering.

(1) Bronstein, L. M.; Chernyshov, D. M.; Volkov, I. O.; Ezernitskaya, M. G.; Valetsky, P. M.; Matveeva, V. G.; Sulman, E. M. *J. Catal.* **2000**, *196*, 302−314.
(2) Sulman, E.; Matveeva, V.; Usanov, A.; Kosivtsov, Y.; Demidenko, G.; Bronstein, L.; Chernyshov, D.; Valetsky, P. *J. Mol. Catal. A: Chem.* **1999**, *146*, 265−269.
(3) Bronstein, L.; Kramer, E.; Berton, B.; Burger, C.; Forster, S.; Antonietti, M. *Chem. Mater.* **1999**, *11*, 1402.
(4) Seregina, M. V.; Bronstein, L. M.; Platonova, O. A.; Chernyshov, D. M.; Valetsky, P. M.; Hartmann, J.; Wenz, E.; Antonietti, M. *Chem. Mater.* **1997**, *9*, 923−931.
(5) Antonietti, M.; E.Wenz; Bronstein, L.; Seregina, M. *Adv. Mater.* **1995**, *7*, 1000.
(6) Ciebien, J. F.; Cohen, R. E.; Duran, A. *Supramol. Sci.* **1998**, *5*, 31−39.
(7) Heilmann, A.; Hamann, C. *Prog. Colloid Polym. Sci.* **1991**, *85*, 102−110.
(8) Bahnemann, D. W. *Isr. J. Chem.* **1993**, *33*, 115−136.
(9) Cummins, C. C.; Schrock, R. R.; Cohen, R. E. *Chem. Mater.* **1992**, *4*, 27−30.
(10) Sohn, B. H.; Cohen, R. E. *J. Appl. Polym. Sci.* **1997**, *65*, 723−729.
(11) Caro, D. d.; Ely, T. O.; Mari, A.; Chaudret, B. *Chem. Mater.* **1996**, *8*, 1987−1991.
(12) Cao, X.; Koltypin, Y.; Kataby, G.; Prozorov, R.; Gedanken, A. *J. Mater. Res.* **1995**, *10*, 2952−2957.
(13) Grinstaff, M. W.; Salamon, M. B.; Suslick, K. S. *Phys. Rev. B: Condens. Matter Mater. Phys.* **1993**, *48*, 269−273.
(14) Kumar, R. V.; Koltypin, Y.; Palchik, O.; Gedanken, A. *J. Appl. Polym. Sci.* **2002**, *86*, 160−165.
(15) Leslie-Pelecky, D. L.; Rieke, R. D. *Chem. Mater.* **1996**, *8*, 1770−1783.
(16) Halperin, W. P. *Rev. Mod. Phys.* **1986**, *58*, 533−606.
(17) Brus, L. E.; Siegel, R. W. *J. Mater. Res.* **1989**, *4*, 704.
(18) Ahmed, S. R.; Ogale, S. B.; Papaefthymiou, G. C.; Ramesh, R.; Kofinas, P. *Appl. Phys. Lett.* **2002**, *80*, 1616−1618.
(19) Sohn, B. H.; Cohen, R. E.; Papaefthymiou, G. C. *J. Magn. Magn. Mater.* **1998**, *182*, 216−224.
(20) Ziolo, R. F.; Giannelis, E. P.; Shull, R. D. *Nanostruct. Mater.* **1993**, *3*, 85−92.
(21) Ziolo, R. F.; Giannelis, E. P.; Weinstein, B. A.; O'Horo, M. P.; Ganguly, B. N.; Mehrotra, V.; Russell, M. W.; Huffman, D. R. *Science* **1992**, *257*, 219−223.
(22) Vassiliou, J. K.; Mehrotra, V.; Russell, M. W.; Giannelis, E. P.; McMichael, R. D.; Shull, R. D.; Ziolo, R. F. *J. Appl. Phys.* **1993**, *73*, 5109−5116.
(23) Sohn, B. H.; Seo, B. H. *Chem. Mater.* **2001**, *13*, 1752−1757.
(24) Sohn, B. H.; Cohen, R. E. *Chem. Mater.* **1997**, *9*, 264−269.
(25) Clay, R. T.; Cohen, R. E. *Supramol. Sci.* **1996**, *2*, 183−191.
(26) Sun, S.; Murray, C. B.; Weller, D.; Folks, L.; Moser, A. *Science* **2000**, *287*, 1989−1992.
(27) Platonova, O. A.; Bronstein, L. M.; Solodovnikov, S. P.; Yanovskaya, I. M.; Obolonkova, E. S.; Valetsky, P. M.; Wenz, E.; Antonietti, M. *Colloid Polym. Sci.* **1997**, *275*, 426−431.
(28) Rutnakornpituk, M.; Thompson, M. S.; Harris, L. A.; Farmer, K. E.; Esker, A. R.; Riffle, J. S.; Connolly, J.; Pierre, T. G. S. *Polymer* **2002**, *43*, 2337−2348.
(29) Smith, T. W.; Wychick, D. *J. Phys. Chem.* **1980**, *84*, 1621−1629.
(30) Dinega, D. P.; Bawendi, M. G. *Angew. Chem., Int. Ed.* **1999**, *38*, 1788−1791.
(31) Hess, P. H., Jr.; P. H. P. *J. Appl. Polym. Sci.* **1966**, *10*, 1915−1927.
(32) Park, S.-J.; Kim, S.; Lee, S.; Khim, Z. G.; Char, K.; Hyeon, T. *J. Am. Chem. Soc.* **2000**, *122*, 8581−8582.
(33) Pathmamanoharan, C.; Philipse, A. P. *J. Colloid Interface Sci.* **1998**, *205*, 340−353.
(34) Bronstein, L.; Chernyshov, D.; Valetsky, P.; Tkachenko, N.; Lemmetyinen, H.; Hartmann, J.; Forster, S. *Langmuir* **1999**, *15*, 83−91.
(35) Ribbe, A. E.; Okumura, A.; Matsushige, K.; Hashimoto, T. *Macromolecules* **2001**, *34*, 8239−8245.
(36) Lee, K. M.; Sorensen, C. M.; Klabunde, K. J.; Hadjipanayis, G. C. *IEEE Trans. Magn.* **1992**, *28*, 3180−3182.
(37) Sidorov, S. N.; Bronstein, L. M.; Davankov, V. A.; Tsyurupa, M. P.; Solodovnikov, S. P.; Valetsky, P. M. *Chem. Mater.* **1999**, *11*, 3210−3215.
(38) Veintemillas-Verdaguer, S.; Morales, M. P.; Cerna, C. J. *Mater. Lett.* **1998**, *35*, 227−231.
(39) Zachariah, M. R.; Aquino, M. I.; Shull, R. D.; Steel, E. B. *Nanostruct. Mater.* **1995**, *5*, 383−392.

10.1021/cm021021q CCC: $25.00 
Published on Web 02/12/2003

**Table 1. P(S-*b*-2VP) Samples from Polymer Source, Inc.**

| code | PS block $M_n$ | P2VP block $M_n$ |
|---|---|---|
| **COP1** | 91 300 | 115 000 |
| **COP2** | 81 000 | 21 000 |

mercially desirable goal of a well-ordered array of monodisperse ferromagnetic nanoparticles for data storage, however, has been difficult. Many syntheses have been unable to produce particles above the superparamagnetic size limit and are therefore not applicable to data storage, which requires a permanent magnetic dipole. Other problems include agglomeration of particles, and irregular particle shapes at particle sizes large enough to show ferromagnetic, rather than superparamagnetic, behavior at room temperature.[13,14,27,28,31,36,40] One research group recently created a lattice of colloidally grown, monodisperse, ferromagnetic FePt particles,[26] but their approach requires deposition on a surface flat enough for self-assembly.

In this paper we report the synthesis of cobalt nanoparticles in the poly(2-vinyl pyridine) domains of films of poly(styrene-*b*-2-vinyl pyridine) by the thermal decomposition of organometallic cobalt. Dicobalt octacarbonyl has been a tool of earlier research efforts,[27,28,30,31,33,37,40,41] and similar polymers have previously been used in nanoparticle synthesis.[1,2,4,23,27,29,34,35] Our research departs from earlier efforts, however, by first making in solution a cobalt organometallic, $[(CO)_4CoCo(Py)_3]^+[Co(CO)_4]^-$, that is selectively sequestered into the poly(2-vinyl pyridine) blocks in useful amounts during solvent casting. The sequestering group, 2-vinyl pyridine, is a weak electron donor; thus, in the present system there is minimal thermodynamic constraint on the growth of the nanoparticles that arises from surface-passivating interactions between polymer-bound ligands and the nanoparticle surfaces. Bulk film processing thus enables the growth of nanoparticles large enough for hard magnetism at room temperature. This method could be useful for flexible data storage media since it allows particles to be formed in particular places in situ; there is no need for dispersion of the particles on a smooth surface.

## Experimental Section

**Materials.** Dicobalt octacarbonyl ($Co_2(CO)_8$) from Strem (Newburyport, MA) was refrigerated under nitrogen. Toluene (99.8%, anhydrous) was obtained from Sigma-Aldrich (St. Louis, MO). Pyridine (99.5+%) was obtained from Alfa Aesar (Ward Hill, MA). Two different samples of poly(styrene-*b*-2-vinyl pyridine) (P(S-*b*-2VP)), **COP1** and **COP2** (see Table 1), were obtained from Polymer Source Inc. (Dorval, Quebec, Canada). All chemicals were used without further purification.

**Synthesis.** To avoid oxidation of $Co_2(CO)_8$, all solutions were made in a Vacuum Atmospheres glovebox in an inert atmosphere ($N_2$). An organometallic stock solution was made by adding 10 mL of pyridine to 0.4 g of $Co_2(CO)_8$ and stirring overnight to allow evolution of CO. The molar ratio of pyridine to cobalt was 106, well in excess of the value of 1 required for the reaction (1) below. Polymer solutions were made by stirring a mixture of 0.2 g of polymer, 10 mL of toluene, and 10 mL of pyridine at temperatures below 110 °C until the polymer dissolved and then allowing the mixture to cool to room temperature. The desired amount of organometallic stock solution was then added. The amount of loading was calibrated to a basis of weight percent $Co_2(CO)_8$ of P2VP block.

Film casting was done in the glovebox with a constant $N_2$ purge to remove evaporated solvent from the glovebox. Polymer solutions were poured into small glass crystallizing dishes or Petri dishes and left until the solvent evaporated (~24−48 h). The resulting films were then dried in a vacuum overnight at room temperature. To decompose the organometallic and make particles, small pieces of film were cut out with a razor blade, sealed in an enclosed vessel to keep them in a pure $N_2$ atmosphere, and heated in a vacuum oven for 24 h at various temperatures ranging from 90 to 210 °C.

**Analysis.** For transmission electron microscopy (TEM) imaging, bulk-cast samples were cut in a direction normal to the film plane using a RMC MT-X ultramicrotome at room temperature with either a diamond knife (Diatome, Fort Washington, PA) or a glass knife. Approximately 50−70-nm-thick cross sections of the samples were obtained. Cut sections were floated onto a trough of deionized water, immediately picked up with copper TEM grids, and blotted dry. TEM was performed on these sections with either a JEOL JEM-2000FX operated at 200 kV or a JEOL JEM-200CX operated at 200 kV. The samples were oriented during TEM so that the electron beam was normal to the plane of the cross section.

Magnetic measurements were made using a Princeton Measurements Corporation MicroMag 2900 Alternating Gradient Magnetometer (AGM).

## Results and Discussion

For the reaction of $Co_2(CO)_8$ with pyridine (Py), Fachinetti et al.[42] found the following:

$$3Co_2(CO)_8 + 6Py \rightarrow 2[(CO)_4CoCo(Py)_3]^+[Co(CO)_4]^- + 8CO\uparrow \quad (1)$$

Upon mixing pyridine and $Co_2(CO)_8$ to form stock solution, we observed bubbling, consistent with CO being evolved by the above reaction. Platonova et al.[27] suggest a similar reaction between $Co_2(CO)_8$ and polymer-bound pyridine groups, indicating the possibility of ligand exchange between cobalt organometallic complexes and these groups.

During the solvent casting of the bulk polymer films, the organometallic complex on the right side of reaction (1) is in the toluene and pyridine solution along with the P(S-*b*-2VP) molecules. As the toluene and pyridine evaporate, this complex is selectively sequestered into the P2VP regions of the mixture, both as a result of enhanced miscibility (solubility parameter considerations) and ligand exchange with the polymer-bound pyridine groups.

The series of micrographs in Figures 1−4 demonstrates this spatial segregation of cobalt within the heterogeneous, nanoscale morphologies of the P(S-*b*-2VP) films. The composition of **COP1** is in the range for which a lamellar morphology is expected[43,44] and Figures 1 and 2 (low amount of added organometallic complex) show the lamellar structure in which the P2VP domains are decorated with cobalt nanoparticles in a dark background. This background staining of the P2VP arises from the presence of a bound cobalt complex that

(40) Tadd, E. H.; Bradley, J.; Tannenbaum, R. *Langmuir* **2002**, *18*, 2378−2384.
(41) Bronstein, L. M.; Mirzoeva, E. S.; Valetsky, P. M.; Solodovnikov, S. P.; Register, R. A. *J. Mater. Chem.* **1995**, *5*, 1197−1201.
(42) Fachinetti, G.; Fochi, G.; Funaioli, T.; Zanazzi, P. F. *Angew. Chem., Int. Ed. Engl.* **1987**, *26*, 680−681.
(43) Noshay, A.; McGrath, J. E. *Block Copolymers: Overview and Critical Survey*; Academic Press, Inc.: New York, 1977.
(44) Sadron, C.; Gallot, B. *Makromol. Chem.* **1973**, *164*, 301.

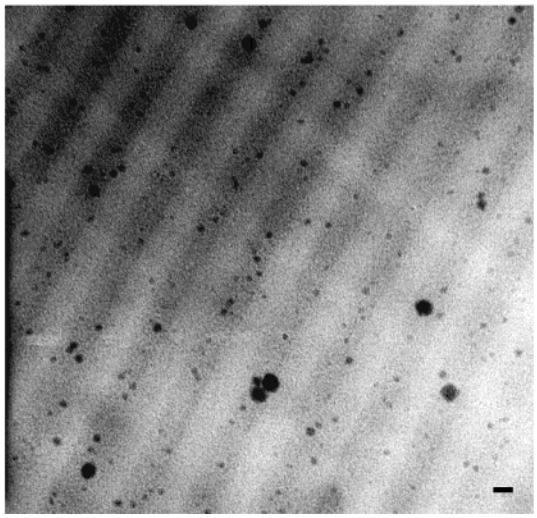

**Figure 1.** Lamellar morphology of solution-cast **COP1**, containing $Co_2(CO)_8$ 10 wt % of P2VP block. The bulk film was heated to 90 °C for 24 h to produce the Co nanoclusters seen in the P2VP domains. Scale bar = 25 nm.

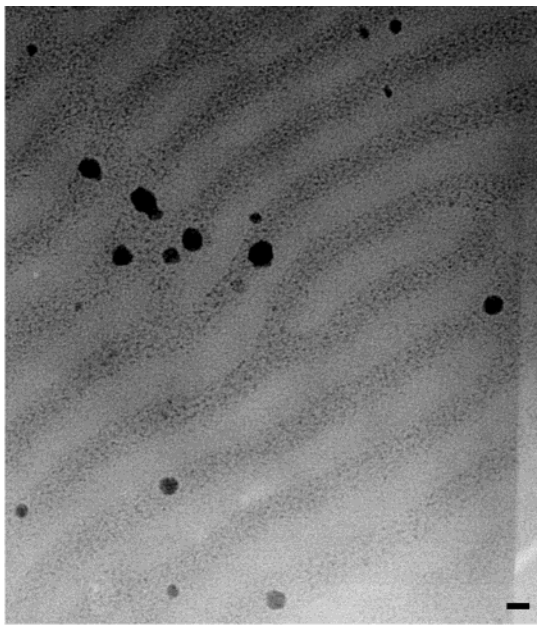

**Figure 2.** Lamellar morphology of **COP1**, containing $Co_2(CO)_8$ 20 wt % of P2VP block heated to 90 °C for 24 h. Scale bar = 25 nm.

has not been incorporated into nanoparticles over the 24-h period at 90 °C. IR spectra of these films show strong absorbances in the range of 1800−2100 $cm^{-1}$ associated with the CO ligands of the complex. In both Figures 1 and 2 the cobalt nanoparticles remain mostly within the P2VP lamellae. It is thermodynamically favorable for them to do so since electron-donating pyridine groups can satisfy the otherwise incomplete bonding at the particle surface.

Figure 3 shows a morphology of PS cylinders embedded in a matrix composed of P2VP and organometallic complex. This morphological transformation arises at larger amounts of added cobalt complex because the complex selectively increases the volume fraction of the P2VP regions beyond the range in which the lamellar morphology can form spontaneously. Upon heating to 90 °C, the Co nanoparticles reside largely outside the

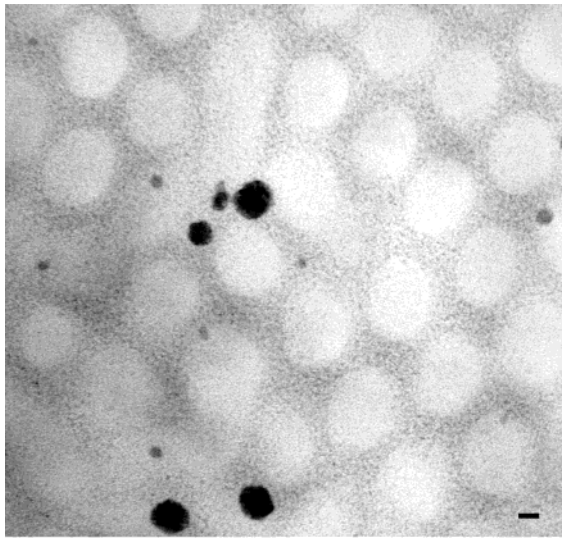

**Figure 3.** Morphology of **COP1**, with $Co_2(CO)_8$ 30 wt % of P2VP block, heated to 90 °C for 24 h. Because the $Co_2(CO)_8$ is selectively sequestered into the P2VP domains, their volume fraction increases relative to the PS domains, resulting in a morphological transformation to PS cylinders embedded in a P2VP and organometallic additive matrix. Scale bar = 25 nm.

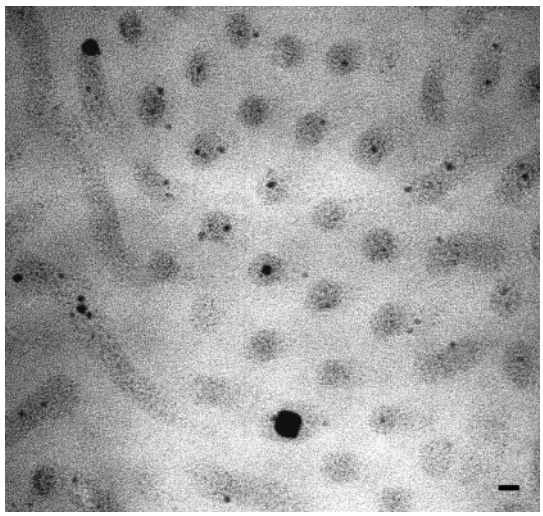

**Figure 4.** Solution-cast **COP2**, with $Co_2(CO)_8$ 20 wt % of P2VP block, heated to 90 °C for 24 h. Because it contains a larger fraction of PS than **COP1** does, **COP2** presents a morphology of P2VP cylinders in a PS matrix. The Co nanoclusters are formed inside the P2VP cylinders. Scale bar = 25 nm.

PS cylinders as expected, although not as clearly defined as in the case of the lamellar structures. Figure 4 shows the P2VP cylindrical morphology of **COP2** and Co nanoparticles residing within the cylindrical P2VP domains.

Some statistical analysis of our full set of micrographs allowed us to derive trends from the particle sizes and size distributions in the various samples. For every specimen a sufficient number of micrographs was examined so that the diameters of 50 particles were measured, leading to histograms of the type shown in Figure 5. Table 2 presents information from these histograms for the full set of specimens and processing conditions. Generally speaking, particle sizes increased with the amount of cobalt complex added to the copolymer and with the temperature used for the decomposi-

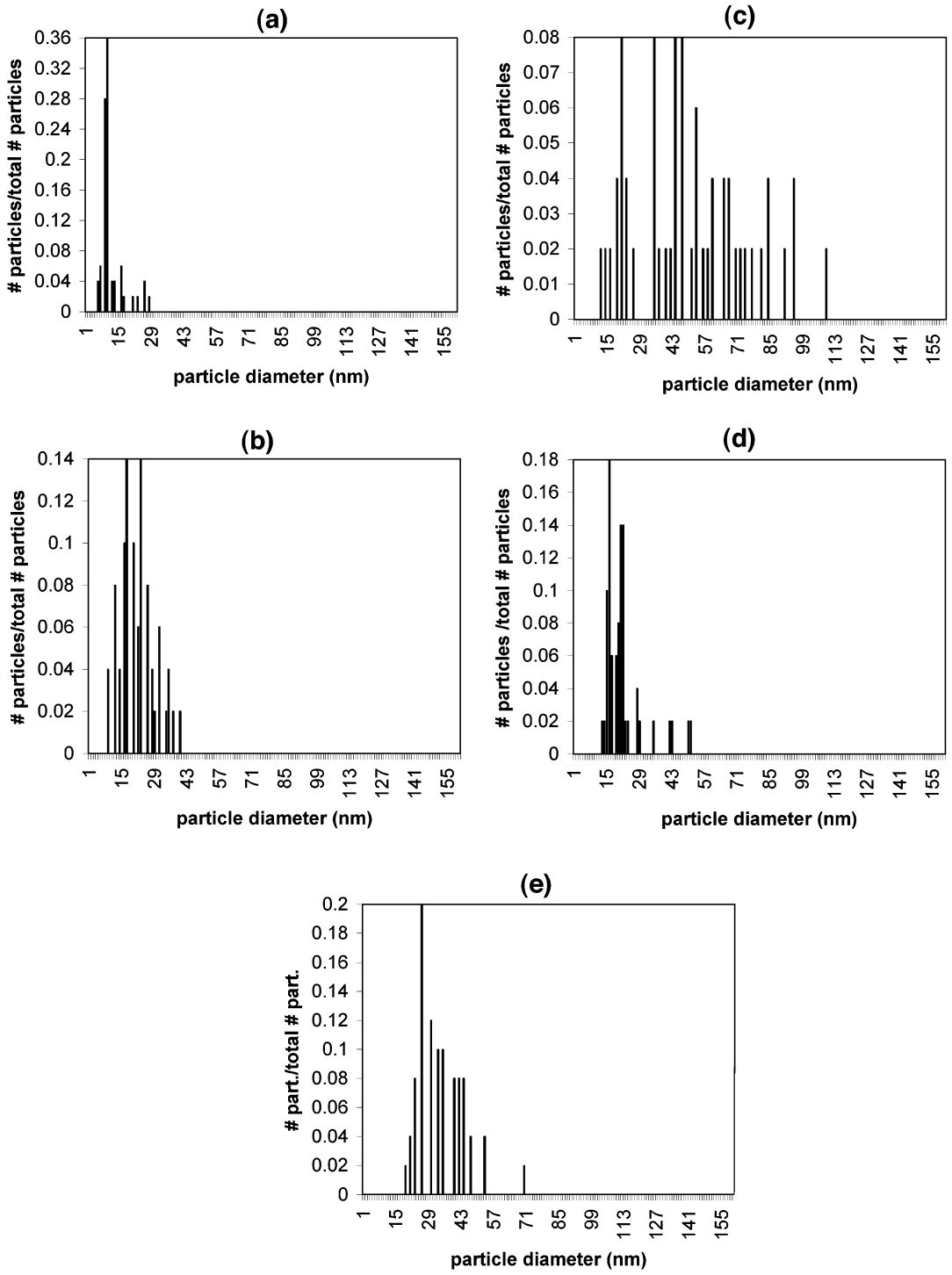


**Figure 5.** Histograms showing the frequency of particles of various sizes in **COP1** films: (a) with $Co_2(CO)_8$ 10 wt % of P2VP block, heated to 90 °C for 24 h; (b) with $Co_2(CO)_8$ 20 wt % of P2VP block, heated to 90 °C for 24 h; (c) with $Co_2(CO)_8$ 30 wt % of P2VP block, heated to 90 °C for 24 h; (d) with $Co_2(CO)_8$ 20 wt % of P2VP block, heated to 170 °C for 24 h; (e) with $Co_2(CO)_8$ 20 wt % of P2VP block, heated to 210 °C for 24 h. Numerous micrographs beyond those shown were used to develop the histograms; 50 particles were sampled for each histogram. Full results are summarized in Table 2.

tion of the complex. Higher loadings led in general to broader distributions, reflected in the value of $D_{max}/D_{mode}$ in Table 2. The particle diameters listed in this table do not represent the size of a single cobalt crystal. Electron diffraction patterns of all the TEM specimens showed diffuse rings and/or spot patterns, suggesting multicrystalline particles. These diffraction patterns could not be used quantitatively to determine the crystal form and crystal size in the various samples.

The nanoparticles, some of which are 100 nm or more in diameter (see Table 2), are significantly larger than the ≤5-nm-diameter nanoparticles produced by many other in-film synthesis methods.[9,11,18,19,24,25,40] In general, nanoclusters in a P2VP domain become more stable as they grow in size because the surface-to-volume ratio decreases, and the number of electron-donating ligands it is in contact with increases.[45] For spherical nanoclusters growing to an equilibrium size

**Table 2. Maximum and Mode of Particle Distributions for Various Copolymers and Processing Conditions**

| polymer type | dicobalt octacarbonyl loading (wt % of P2VP block) | processing temperature (°C) | $D_{max}$ (nm) | $D_{mode}$ (nm) | $D_{max}/D_{mode}$ |
|---|---|---|---|---|---|
| **COP1** | 30 | 90 | 109 | 47 | 2.3 |
| **COP1** | 30 | 130 | 74 | 47 | 1.6 |
| **COP1** | 30 | 170 | 170 | 53 | 3.2 |
| **COP1** | 30 | 210 | 174 | 35 | 5.0 |
| **COP1** | 20 | 90 | 40 | 23 | 1.7 |
| **COP1** | 20 | 130 | 63 | 44 | 1.4 |
| **COP1** | 20 | 170 | 51 | 16 | 3.2 |
| **COP1** | 20 | 210 | 70 | 26 | 2.7 |
| **COP2** | 30 | 90 | 130 | 126 | 1.0 |
| **COP2** | 30 | 130 | 42 | 42 | 1.0 |
| **COP2** | 30 | 170 | 38 | 16 | 2.4 |
| **COP2** | 30 | 170 | 288 | 153 | 1.9 |
| **COP2** | 30 | 210 | 153 | 119 | 1.3 |
| **COP1** | 10 | 90 | 28 | 10 | 2.8 |
| **COP2** | 20 | 90 | 35 | 10 | 3.5 |

within the polymer film,

$$KR_p^2/(\#LCs)_r = \text{constant}$$

where $K$ is the equilibrium constant of the ligand−nanocluster reaction, $(\#LCs)_r$ is the number of ligand−nanocluster bonds required for thermodynamic stability, and $R_p$ is the nanocluster radius.[45] Since our sequestering group, pyridine, is a much weaker electron donor than the groups (e.g., carboxylate, sulfonate, and TOPO) used by other researchers,[9,11,18−22,24,25,30,40] the stabilizing effect of electron donation in our films is smaller, and therefore, $(\#LCs)_r$ is larger. In the present work, $K$ should be small, again because pyridine is a weak electron donor. $R_p$ would then have to be larger, to keep the overall term on the left constant.

It is apparent from the dark background in the P2VP domains of Figures 1−4 that the 90 °C, 24-h heating cycle does not lead to full conversion of the sequestered cobalt complex into metallic cobalt nanoclusters. As indicated in Table 2, we used a variety of temperatures above 90 °C in an attempt to utilize the loaded cobalt more efficiently. Magnetic measurements discussed below indicate that a greater fraction of the sequestered cobalt is converted to metallic clusters as the temperature of the heating cycle was increased. Microscopic evidence for this statement is shown in Figure 6, where the cobalt nanoclusters formed in **COP1** at 170 °C appear at high concentration in P2VP domains, with only a minimum of residual staining from unconverted complexed cobalt (compare Figures 6 and 2).

Magnetic properties of the nanocomposite block copolymer films revealed a strong dependence on particle size. The Co nanoparticles are ferromagnetic at room temperature, with coercivities up to 360 Oe. Some representative hysteresis loops, measured using AGM within a day of particle formation, are shown in Figure 7. The cobalt nanoparticles are quite stable to oxidative degradation as shown in Figure 8. An AGM measurement of an approximately 11-month old sample stored in a laboratory atmosphere, when compared to an AGM measurement taken just after the sample was made, shows that the particles lose little in the way of remanence or coercivity with time. This may be because the pyridine groups of the P2VP bind to the particles' surfaces, as discussed above, and lower their surface energy, making them less prone to oxidation. A similar effect was observed by Dinega and Bawendi with TOPO ligands.[30]

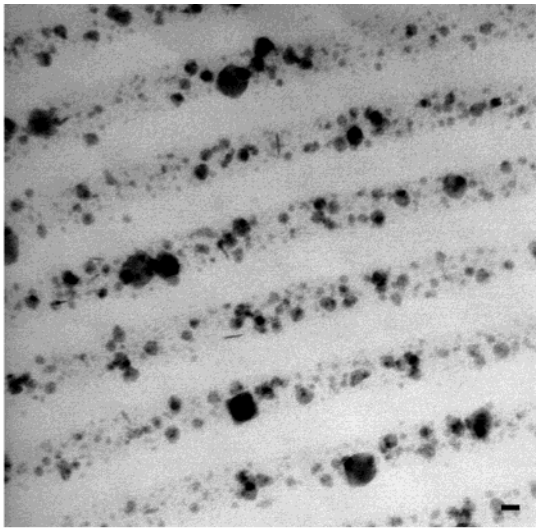

**Figure 6.** Lamellar morphology of **COP1**, containing $Co_2(CO)_8$ 20 wt % of P2VP block heated to 170 °C for 24 h. Scale bar = 25 nm.

The normalized saturation magnetization (emu/g of P2VP) for each level of cobalt loading shows a strong positive correlation with the temperature used to decompose the sequestered organometallic complex (see Figure 9). This confirms the postulate, based on TEM evidence shown above, that as the particle formation temperature increases, more of the organometallic complex is converted into magnetic particles, leading to a higher volume fraction of Co. At the highest temperature of particle formation used, 210 °C, this conversion is complete to within experimental error. On the basis of literature values[46] for cobalt of 1420 emu/cm$^3$ for $M_s$ and 8.92 g/cm$^3$ for density, the saturation magnetization for **COP1** 30% for complete conversion, for example, should be 23.5 emu/g of P2VP. The experimentally observed value is 26.0 emu/g of P2VP (see Figure 9). Furthermore, at this temperature, the saturation magnetization of the **COP1** 20% loaded sample is approximately two-thirds that of the **COP1** 30%

(45) Kane, R. S.; Cohen, R. E.; Silbey, R. *Langmuir* **1999**, *15*, 39−43.

(46) Cullity, B. D. *Introduction to Magnetic Materials*; Addison-Wesley Publishing Co.: Reading, MA, 1972.

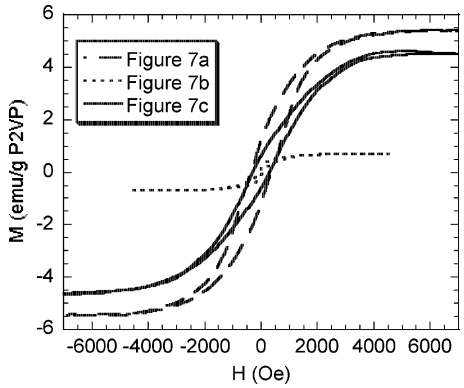


**Figure 7.** Magnetization ($M$) vs applied magnetic field ($H$) AGM curves of bulk-cast samples, taken at room temperature. Since a small but unknown amount of cobalt does not react in each sample, the $y$-axis was normalized to the mass of the P2VP domains in the sample being measured, for consistency. (a) **COP1**, with $Co_2(CO)_8$ 30 wt % of P2VP block, heated to 90 °C for 24 h. Coercivity ($H_c$) = 360 Oe, remanent magnetization ($M_r$) = 1.2 emu/g P2VP, saturation magnetization ($M_s$) = 5.4 emu/g P2VP. (b) $M$ vs $H$ AGM curve of bulk-cast **COP1**, with $Co_2(CO)_8$ 20 wt % of P2VP block, heated to 90 °C for 24 h. $H_c$ = 68 Oe, $M_r$ = 0.16 emu/g P2VP, $M_s$ = 0.70 emu/g P2VP. (c) $M$ vs $H$ AGM curve of bulk-cast **COP2**, with $Co_2(CO)_8$ 30 wt % of P2VP block, heated to 90 °C for 24 h. $H_c$ = 300 Oe, $M_r$ = 0.63 emu/g P2VP, $M_s$ = 4.6 emu/g P2VP.

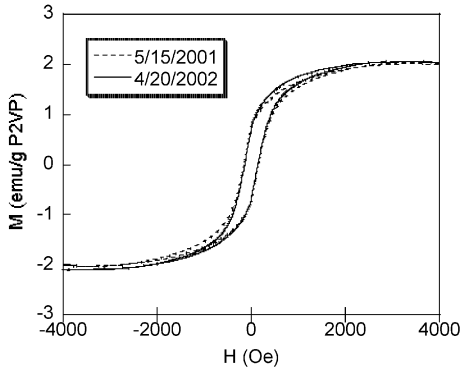


**Figure 8.** (a) Room-temperature $M$ vs $H$ AGM curve of bulk-cast **COP1** from pure pyridine with $Co_2(CO)_8$ 22.6 wt % of P2VP block, heated to 90 °C for 24 h. Date of heating and measurement: 5/15/01. $H_c$ = 140 Oe, $M_r$ = 0.70 emu/g P2VP, $M_s$ = 2.0 emu/g P2VP. (b) Room-temperature $M$ vs $H$ AGM curve of same sample. Date of measurement: 4/20/02. $H_c$ = 140 Oe, $M_r$ = 0.70 emu/g P2VP, $M_s$ = 2.0 emu/g P2VP.

loaded sample, as expected. At lower temperatures, saturation magnetization may not rise monotonically with loading (see, for example, Figure 7) due to incomplete conversion.

Figure 10 shows that there is a gradual decrease in coercivity with the particle formation temperature and a strong increase in coercivity with the level of organometallic loading. To help interpret these results, Figure 11 shows the correlation between coercivity and particle size ($D_{max}$). Higher coercivity is generally associated with larger particle sizes. This is often explained as a result of thermally assisted magnetization reversal, which typically lowers the coercivity of smaller particles. However, as we will show below, the magnetization activation volume is similar for samples grown at different temperatures, and also there does not appear to be a strong correlation between measured particle size and coercivity within a given temperature series,

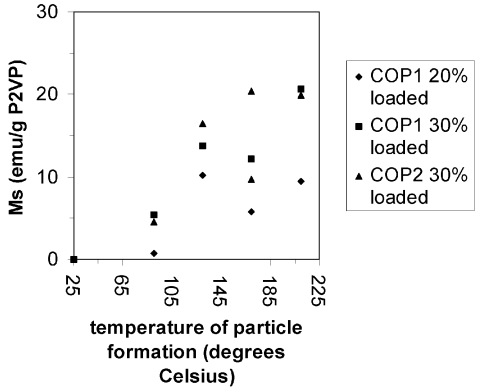


**Figure 9.** $M_s$ vs temperature of particle formation for various samples.

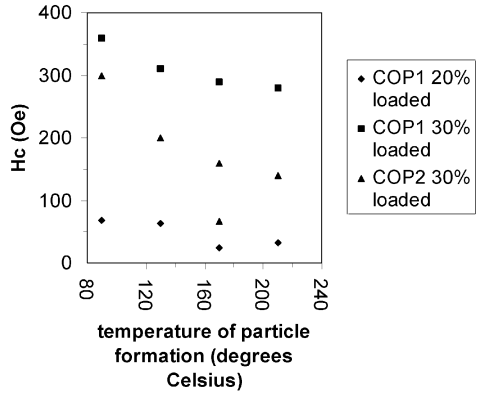


**Figure 10.** $H_c$ vs temperature of particle formation for various samples.

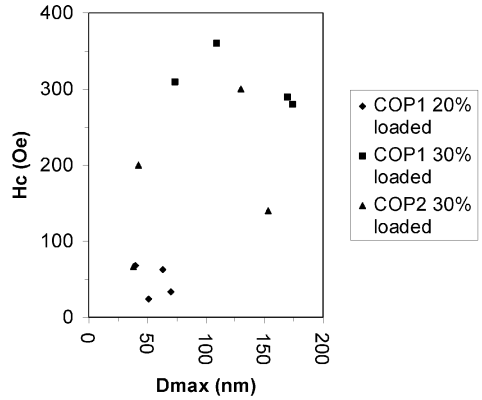


**Figure 11.** $H_c$ vs maximum particle diameter for various samples.

for the same polymer and loading fraction. Instead, the variation in coercivity with processing temperature might reflect a change in particle size distribution or a change in microstructure of the particles. In systems such as these, with well-separated particles having a wide dispersion of diameters, the hysteresis loop is a superposition of the loops of individual particles with a range of coercivities and anisotropy directions. The coercivity of the collective loop represents the field at which half of the net magnetization has reversed. The largest particles, which contain most of the volume of cobalt, contribute disproportionately to the signal, and so changes in coercivity of the ensemble may be a result of small changes in size distribution or microstructure of these larger particles, which may not be apparent

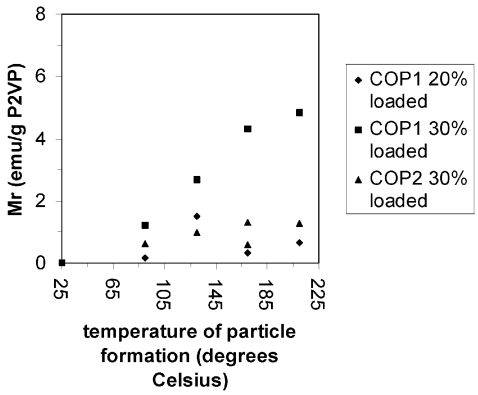


**Figure 12.** $M_r$ vs temperature of particle formation for various samples.

**Table 3. Estimated Activation Volumes for Thermally Assisted Switching of Nanoparticles in Heated Samples, from AGM *M* vs *H* Curves**[a]

| code | wt % carbonyl in P2VP block | temp of particle formation | activation volume ($cm^3$) | diameter of activation volume (nm) |
|---|---|---|---|---|
| **COP1** | 20 | 90 °C | $1.03 \times 10^{-17}$ | 27.0 |
| **COP1** | 20 | 210 °C | $1.20 \times 10^{-17}$ | 28.4 |
| **COP1** | 20 | 130 °C | $7.38 \times 10^{-18}$ | 24.2 |
| **COP1** | 20 | 170 °C | $1.02 \times 10^{-17}$ | 26.9 |
| **COP1** | 30 | 210 °C | $2.61 \times 10^{-17}$ | 36.8 |

[a] A diameter has been calculated for each activation volume for comparison with Table 2. Five AGM runs were performed for each sweep rate.

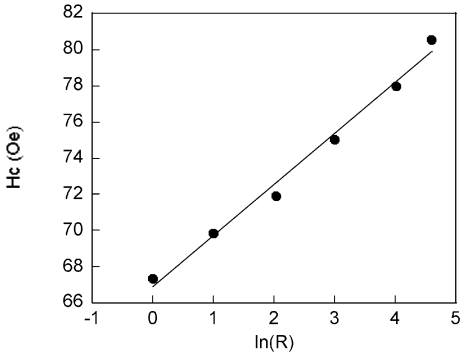


**Figure 13.** Plot of coercivity as a function of the logarithm of the sweep rate, *R*, for **COP1** containing $Co_2(CO)_8$ 20 wt % of P2VP block heated to 170 °C for 24 h.

from the statistical data of Figure 5. Nevertheless, Figure 11 suggests that the conditions used during the in situ synthesis of cobalt nanoparticles can be used to control the coercivity of the nanocomposite films over a range of up to ~350 Oe. One other point to note is that these samples typically have a low remanence (see Figure 12), as a result of the distribution of anisotropy axis directions within the ensemble, and the presence of superparamagnetic particles.

The time-dependent behavior of several samples was examined, using AGM, by measuring room-temperature hysteresis loops at different sweep rates *R* (*R* is the rate of change of the applied field). The activation volume *V** for thermally assisted switching is found by curve-fitting data to the equation $H_c(R) = C + (k_BT/M_sV^*)\ln(R)$ (see Table 3 and Figure 13).[47] In this expression, *C* is a constant, $k_B$ is Boltzmann's constant, *T* is the temperature, and *V** represents the volume of material within a particle that has to reverse in order to cause complete reversal of the particle's magnetic dipole moment. A literature value[46] of 1420 emu/$cm^3$ was used for $M_s$. In the present case, the interpretation is made more difficult by the wide size distribution of the Co particles, but if we assume that the larger particles dominate the hysteresis behavior, then from Tables 2 and 3 the effective magnetic diameters found from *V** are much smaller than the maximum particle diameters found in our micrographs. This suggests that the reversal occurs nonuniformly, that is, the reversal is initiated within a fraction of the particle volume. This reversing volume could for instance be a grain within a polycrystalline particle. Similar behavior has been found for lithographically patterned, polycrystalline Ni particles[48] in which the activation volume was identified with the columnar grains within the particles. The data on the Co composites also indicates that the particles are magnetically isolated, as expected from their wide separation, since interacting magnetic particles would display an effective volume larger than that of an individual particle.[49]

**Acknowledgment.** We thank Michael Frongillo at MIT for his help with transmission electron microscopy and Joy Cheng at MIT for her help with AGM. This work was supported in part by the MRSEC Program of the National Science Foundation under award number DMR 98-08941, and we made use of shared experimental facilities at the MIT Center for Materials Science and Engineering.

CM021021Q

(47) Bruno, P.; Bayreuther, G.; Beauvillain, P.; Chappert, C.; Lugert, G.; Renard, D.; Renard, J. P.; Seiden, J. *J. Appl. Phys.* **1990**, *68*, 5759−5766.

(48) Ross, C. A.; Chantrell, R.; Hwang, M.; Farhoud, M.; Savas, T. A.; Hao, Y.; Smith, H. I.; Ross, F. M.; Redjdal, M.; Humphrey, F. B. *Phys. Rev. B: Condens. Matter Mater. Phys.* **2000**, *62*, 14252−14258.

(49) Cheng, J. Y.; Ross, C. A.; Thomas, E. L.; Smith, H. I.; Lammertink, R. G. H.; Vancso, G. J. *IEEE Magn.* **2002**, *38*, 2541−2543.